Molecular simulation of the vapor-liquid phase behavior of Lennard-Jones mixtures in porous solids

John K. Brennan* and Wei Dong

*Institut de Recherche sur la Catalyse, Centre National de la Recherche Scientifique, Group de Chimie Theorique,
2 Avenue Albert Einstein, 69626 Villeurbanne Cedex, France
and Group de Chimie Theorique, Ecole Normale Superieure de Lyon, 46 Allee d'Italie, 69364 Lyon, Cedex 07, France*

We present vapor-liquid phase coexistence curves for binary fluid mixtures in a disordered porous solid. The porous material is modeled as a collection of randomly dispersed hard spheres. A variant of the Monte Carlo Gibbs ensemble method [J. K. Brennan and W. Dong, J. Chem. Phys. **116**, 8948 (2002)] is used to simulate Lennard-Jones fluid mixtures at several porosities: 0.9, 0.95, and 0.975. Effects based on the size and the energetics of the mixture components are studied. Pressure-composition and pressure-density phase diagrams at reduced temperatures of 0.75 and 1.0 are reported. Compared to the bulk fluid behavior, dramatic shifts in the phase envelope were found for even highly porous structures. Both the Lennard-Jones size and energy mixture parameters were found to strongly influence the resulting shape of the phase envelope.

I. INTRODUCTION

Knowledge of the phase behavior of fluids adsorbed in porous materials is essential for optimizing current chemical processes and for the invention of nanoscale technologies and materials. Compared to the bulk fluid, drastic shifts and reductions of the phase envelope have been found to occur for pure fluids confined in porous solids [1–5]. Challenges encountered when studying confined fluids in the laboratory as well as inconsistent theoretical results suggest the need for a concerted effort that includes experimental, theoretical, and simulation approaches. The difficulty of simulating the phase transitions of confined fluids is evidenced by the plethora of studies carried out in idealized geometries (e.g., slits and cylinders). Using molecular simulation to trace true coexistence curves of fluids in more complex porous solids has been limited to pure fluids [2–5] and symmetric liquid-liquid mixtures [6]. In recent work [5], a variant of the Gibbs ensemble method was shown to be an efficient technique for simulating the phase behavior of fluids confined in random porous solids. The efficacy of the method allowed for a systematic study of a pure Lennard-Jones fluid in a variety of porous solid models.

An important industrial application of porous materials is in the various separation and purification processes. For these technologies, an engineer most often requires knowledge of the phase behavior of fluid *mixtures* in porous materials. The difficult task of measuring the composition within the porous material has thus far thwarted attempts to study the vapor-liquid equilibria of mixture systems in the laboratory. Likewise, to date, there have been no successful theoretical predictions of the phase behavior of fluid mixtures

confined in nonidealized pore geometries. Clearly there is a need for molecular simulation studies of confined fluids to provide guidance in developing theories as well as to provide insight into phenomenological trends.

Using a variant of the Gibbs ensemble method introduced previously [5], we have determined vapor-liquid phase diagrams for three model binary mixtures in disordered porous solids. The porous material is modeled as a collection of randomly dispersed hard spheres, while the fluid is a Lennard-Jones mixture. Binary mixtures with components that differ in the Lennard-Jones energy (ε) and size (σ) parameters are simulated at several porosities. Significant reductions in the pressure-composition and pressure-density phase diagrams are found when compared to the bulk fluid mixture phase envelope.

II. SIMULATION MODELS AND METHOD

The fluids are modeled as single-site Lennard-Jones (LJ) particles interacting through the standard (12-6) potential

$$U_{ij}(r) = 4\varepsilon_{ij}\left[\left(\frac{\sigma_{ij}}{r}\right)^{12} - \left(\frac{\sigma_{ij}}{r}\right)^{6}\right], \quad (1)$$

where U_{ij} is the interaction energy between a molecule of species i and a molecule of species j separated by a distance r. The characteristic Lennard-Jones energy (ε_{ij}) and size (σ_{ij}) parameters for the three mixtures studied in this work are given in Table I. Mixtures I and II are intended to isolate

TABLE I. Lennard-Jones potential parameters for the mixtures simulated in this study. Lorentz-Berthelot combining rules were implemented. σ_{11} and ε_{11} were set to unity.

Mixture	σ_{11}	σ_{12}	σ_{22}	ε_{11}	ε_{12}	ε_{22}
I	1.0	0.75	0.5	1.0	1.0	1.0
II	1.0	1.0	1.0	1.0	0.71	0.5
III	1.0	0.875	0.75	1.0	0.71	0.5

*Author to whom correspondence should be addressed. Present address: Weapons and Materials Research Directorate, U.S. Army Research Laboratory, Building 4600, Aberdeen Proving Ground, MD 21005. Electronic address: jbrennan@arl.army.mil

the effects of the size and energy parameters on the phase envelope, respectively, while the parameters for mixture III were chosen to examine a combination of these effects. The Lorentz-Berthelot combining rules have been used, where

$$\varepsilon_{ij} = \sqrt{\varepsilon_{ii}\varepsilon_{jj}} \quad \text{and} \quad \sigma_{ij} = \frac{\sigma_{ii} + \sigma_{jj}}{2} \qquad (2)$$

and the LJ parameters of species 1, σ_{11} and ε_{11}, have been set to unity. The choices of the LJ parameters for these mixtures were predicated on the bulk fluid behavior, which was determined from a Lennard-Jones equation of state [7]. The choice of the parameters for all three mixtures resulted in bulk phase coexistence curves that did not exhibit azeotropic behavior and had reasonably large tie lines.

The porous material is modeled as a collection of randomly dispersed, nonoverlapping hard spheres. The diameter of the hard spheres (σ_s) was chosen such that $\sigma_s = \sigma_{11}$. For this study, the choice of σ_s as well as the nonattractive behavior of the solid particles is intended to isolate the effect of confinement on the phase envelope. The random porous structures were generated by relaxing a face-centered cubic lattice configuration in a Monte Carlo canonical ensemble simulation at the porosity (γ) of interest. We define the porosity for this model in typical fashion as $\gamma = 1 - \eta$, where η is the volume fraction of the hard spheres. Although the model is not intended to mimic any specific porous material, the resulting pore structures are reasonable representations of aerogels and xerogels. For the high values of porosities studied here ($\gamma = 0.9$–0.975), the model structures more closely exhibit aerogel-like behavior.

The details of the Gibbs ensemble method as applied to simulating fluid phase behavior in porous solids are given in the original work [5] and only a brief review is given here. The standard Gibbs ensemble moves of fluid particle displacements and transfers are performed in the two simulation cells representing the coexisting phases. Each fluid simulation cell resides within a porous structure whose volume is significantly larger than the fluid cell volume. A schematic of a simulation cell representing one of the coexisting phases is shown in Fig. 1. Periodic boundary conditions imposed on the fluid particles correspond to the fluid simulation cell. Only the boundaries of the fluid and porous-structure cells behave independently; all other aspects of the cells are correlated. Standard volume expansions and contractions are performed on the fluid simulation cells while the hard spheres making up the porous structures remain fixed. Since the volume of the porous structure is much larger than the fluid simulation cell, fluctuations of the fluid cell volume are always contained within the porous structure. Note that under these conditions the porosity of the porous structure within each fluid simulation cell will not rigorously remain constant. This effect has been thoroughly tested for the pure Lennard-Jones fluid in similar porous models [5]. The porosity in each fluid cell was shown to fluctuate about an average value that differed by less than 4%. No effect of a fluctuating porosity value on achieving the true equilibrium state was found. Lastly, the additional degree of freedom allotted by the phase rule permits either constant-volume or constant-
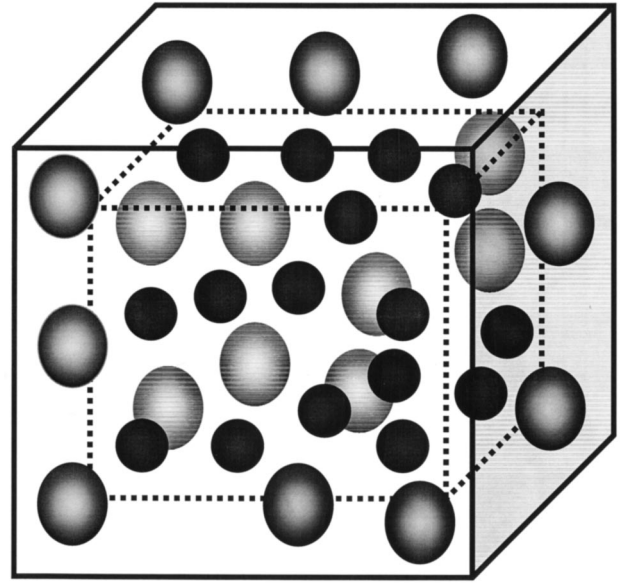

FIG. 1. A schematic of a simulation cell representing one of the coexisting phases. Fluid particles are shown as black spheres while solid particles making up the pore structure are represented as gray spheres. The simulation cell shown as a solid line is rigid and remains fixed, while the simulation cell shown as a dashed line is allowed to expand and contract. Periodic boundary conditions are enforced on the fluid particles for this smaller, flexible cell so that fluid particles always reside in this cell.

pressure Gibbs ensembles to be simulated for mixture systems. We opted to use the constant-pressure version of the Gibbs ensemble method throughout this work, where the pressure reported for all data is the pressure imposed in the acceptance criteria expression for a simulation cell volume change [8].

A minimum of 1500 fluid particles (N_f) in cubic simulation cells was used throughout this study, where standard periodic boundary conditions and the minimum image convention [9,10] were implemented. The simulation cell lengths were typically $12\sigma_{11}$–$15\sigma_{11}$. A potential spherical cutoff of $3.0\sigma_{11}$ was used when calculating all interactions without applying long-range corrections. All the calculated quantities were reduced by the fluid potential parameters of species 1, ε_{11} and σ_{11}.

Initial configurations of the fluid particles were generated by randomly inserting the particles into the fluid simulation cells (without overlap of fluid particle diameters with solid particle diameters) at conditions suspected to be in the two-phase region, followed by a number of fluid particle displacements intended to relax the system. The simulations were performed in cycles, where an average cycle consisted of N_f attempted displacements, a few attempted volume changes, and a number of attempted fluid particle interchanges between the simulation cells representing the coexisting phases. The number of attempted interchanges was selected to result in an acceptance of about 3% of the number of fluid particles of each species being interchanged in each cell during one cycle. The maximum displacement was adjusted to result in a 50% acceptance ratio of the attempted

displacement moves. The maximum change in the simulation cell lengths was adjusted to result in an acceptance ratio of 50% of the attempted volume changes. Typically, 5×10^6 configurations were generated for the equilibrium run and 5×10^7 configurations were generated for the production run. Uncertainties were calculated using the method of block averages [9] where the reported uncertainties correspond to one standard deviation of these block averages.

The simulated results of the confined fluid were compared to bulk fluid phase diagrams predicted from a Lennard-Jones equation of state (EOS) [7] that has been shown to give satisfactory predictions of the phase behavior for a wide variety of mixtures [7,11]. The EOS curves are corrected for the same spherical cutoff ($r_c = 3.0\sigma_{11}$) used in the simulations, again without applying long-range corrections. The van der Waals one-fluid (vdW1f) approximation is used when predicting the bulk fluid phase envelope for the mixtures. The vdW1f approximation considers the properties of the mixture to be those of a single, hypothetical pure fluid. The mixture parameters are taken as [12]

$$\sigma_m^3 = \sum_i \sum_j x_i x_j \sigma_{ij}^3 \quad \text{and} \quad \varepsilon_m = \frac{1}{\sigma_m^3} \sum_i \sum_j x_i x_j \varepsilon_{ij} \sigma_{ij}^3, \tag{3}$$

where x_i is the mole fraction of component i and the double summation is over all the components of the mixture. The vdW1f approximation has been demonstrated to be a good approximation for simple mixtures as well as mixtures with considerable asymmetry in the energy and size parameters [11].

III. RESULTS

We present results for the three Lennard-Jones mixtures specified in Table I at different porosities 0.9, 0.95, or 0.975 and different reduced temperatures $T^* = kT/\varepsilon_{11} = 0.75$ or 1.0 (where k is the Boltzmann constant). The first mixture we consider, mixture I, is composed of fluid particles with different sizes ($\sigma_{11} > \sigma_{22}$) while the energy parameters are equivalent ($\varepsilon_{11} = \varepsilon_{22}$). The specified Lennard-Jones parameters of mixture I are intended to examine the effects of the size of the mixture components on the phase envelope. The porosity of the solid structure is $\gamma = 0.95$. Shown in Fig. 2 is the pressure-composition (P^*-x_1) phase diagram for mixture I at a reduced temperature of $T^* = 1.0$. The reduced pressure is taken as $P^* = P\sigma_{11}^3/\varepsilon_{11}$ and the composition is taken as a number fraction $x_1 = N_1/(N_1 + N_2)$ where N_1 and N_2 are the numbers of particles of species 1 and species 2, respectively. Also shown is the bulk fluid phase diagram predicted from a Lennard-Jones EOS [7]. (The lack of closure of the bulk fluid phase envelope at the critical point is an artifact of the LJ EOS.) Compared to the bulk fluid, the two-phase region of the confined mixture has been reduced. Simulations at reduced pressures above $P^* = 0.2$ did not phase separate, implying that the critical pressure (P_c) for the confined fluid is approximately 30% lower than for the corresponding bulk fluid. Notice too that the P^*-x_1 phase diagram exhibits a shift to lower x_1 values. A physical inter-
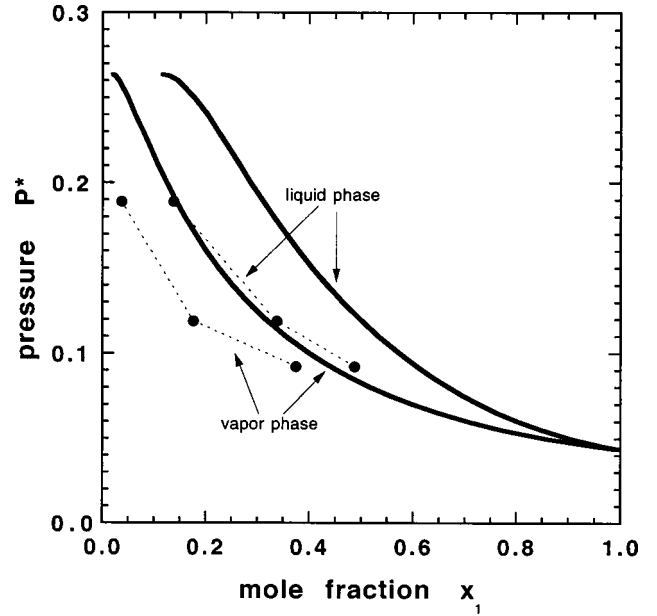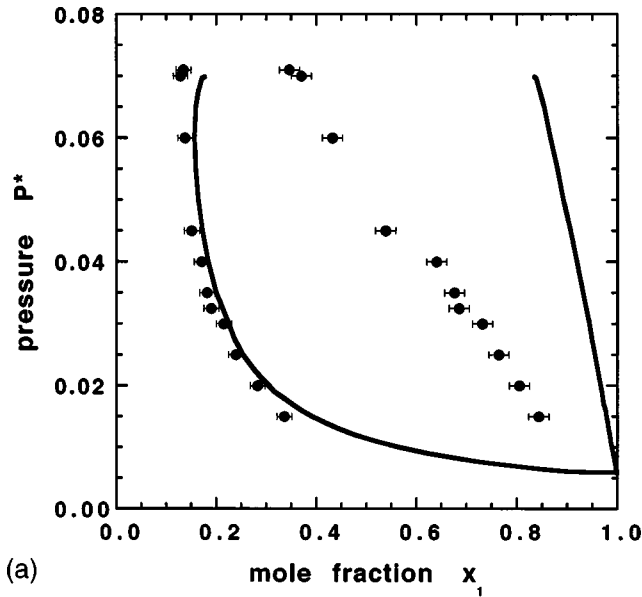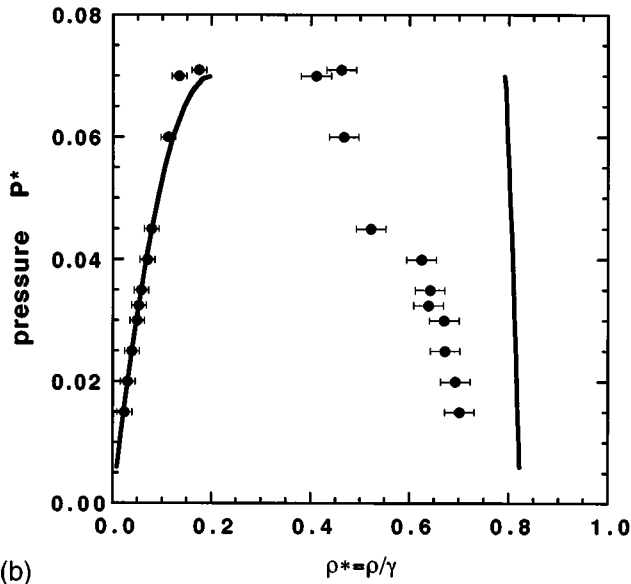

FIG. 2. Pressure-composition phase diagram for mixture I at $T^* = kT/\varepsilon_{11} = 1.0$. The porosity of the solid structure is $\gamma = 0.95$. The reduced pressure is defined as $P^* = P\sigma_{11}^3/\varepsilon_{11}$. The composition is defined as a number fraction $x_1 = N_1/(N_1 + N_2)$ where N_i is the number of particles of species i. The solid line corresponds to the bulk fluid phase behavior determined by a Lennard-Jones EOS [7]. The upper line and upper set of points correspond to the liquid phase, while the lower line and lower set of points correspond to the vapor phase. Error bars (standard deviations determined from block averaging [9]) are smaller than the size of the data points.

pretation for this behavior is that the smaller sized species-2 particles can access the more confined regions of the porous structure which species-1 particles cannot. Interestingly, the breadths of the two-phase region of the confined fluid and the bulk fluid are quite similar. The relative species concentrations of the fluid have changed under confinement but the phase separation mechanism has not. This is expected, however, since the driving force of the phase separation (the attraction between the fluid particles) is the same, i.e., $\varepsilon_{11} = \varepsilon_{22}$. And, although the smaller sized species-2 particles are able to occupy the more confined regions of the porous solid there is no preference for drawing more species-2 particles into these spaces over species-1 particles. For mixtures II and III where $\varepsilon_{11} \neq \varepsilon_{22}$, we find (compared to the bulk fluid) that both the relative species concentrations as well as the two-phase region are altered since attractive forces draw like species into the pore spaces.

The next fluid mixture we studied, mixture II, has particles of equal size ($\sigma_{11} = \sigma_{22}$) while the energy parameter values dictate that species-2 particles have a greater affinity for species-1 particles than for themselves ($\varepsilon_{12} > \varepsilon_{22}$). The Lennard-Jones parameters for mixture II were suitably chosen to isolate effects based on the energetics of the mixture components. P^*-x_1 and P^*-ρ^* phase diagrams of mixture II for $\gamma = 0.975$ at $T^* = 0.75$ are given in Fig. 3. The confined fluid density ($\rho^* = N_f/V_{\text{fluid cell}}$) in Fig. 3(b) has been adjusted by the porosity ($\rho^* = \rho^*/\gamma$) so that a meaningful comparison can be made to the bulk fluid phase diagram [2].
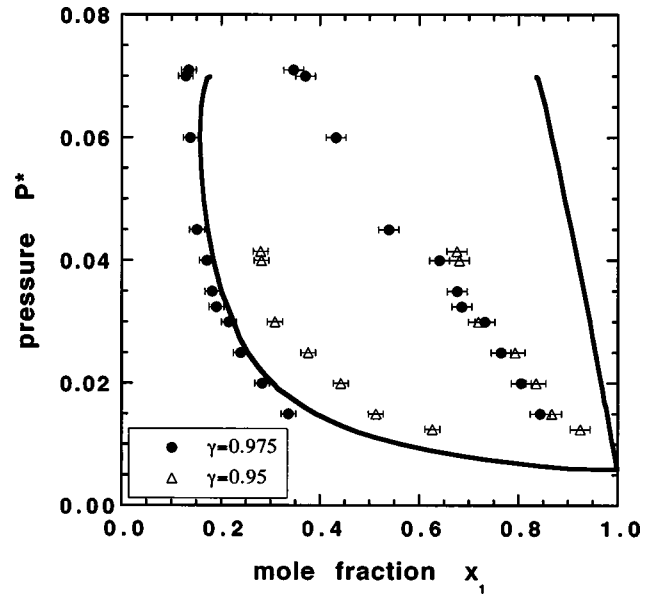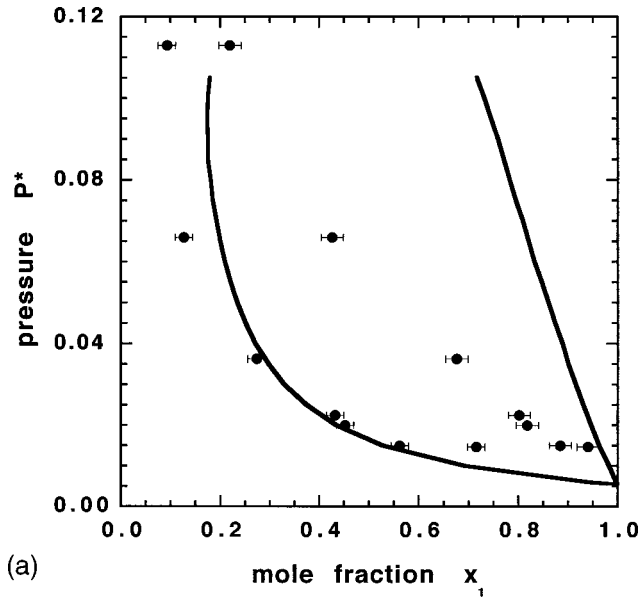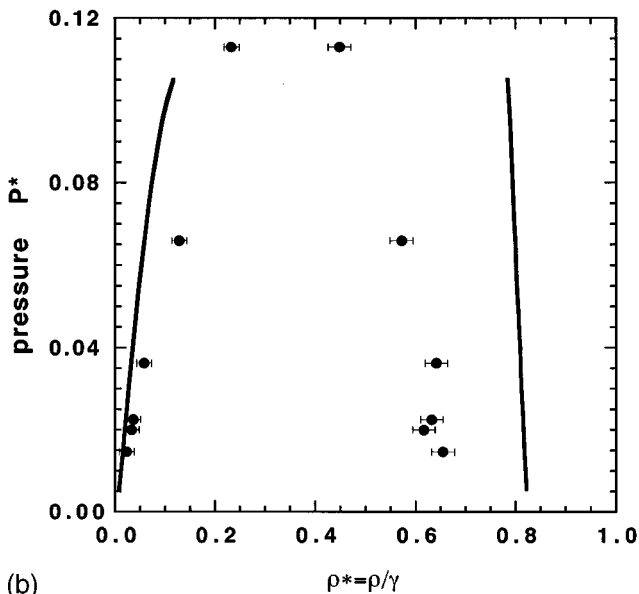
FIG. 4. Pressure-composition phase diagram for mixture II at $T^*=0.75$. Two different porosities $\gamma=0.975$ (●) and $\gamma=0.95$ (△) are shown. Further details are the same as in Fig. 3.

FIG. 3. Pressure-composition (a) and pressure-density (b) phase diagrams for mixture II at $T^*=0.75$. The porosity of the solid structure is $\gamma=0.975$. The reduced pressure is defined as $P^* =P\sigma_{11}^3/\varepsilon_{11}$. The confined fluid density is adjusted for comparison to the bulk fluid by $\rho^*=\rho^*/\gamma=(N_f/V_{\text{fluid cell}})/\gamma$. The corresponding bulk fluid phase behavior is also shown [7]. Error bars are standard deviations determined from block averaging [9].

Both phase diagrams exhibit considerable reductions in the two-phase region. The apparent critical pressures of the bulk and confined mixtures are similar, but the liquid phase boundary of the confined fluid has shifted significantly to lower densities. A general physical interpretation of this behavior is that the discontinuity of the space available to the fluid mixture inside the porous material reduces the cohesive forces and the likelihood that condensation will occur [2,6]. We have also studied the phase behavior of mixture II at a lower porosity of $\gamma=0.95$. A comparison of the P^*-x_1 phase diagrams for $\gamma=0.975$ and 0.95 is given in Fig. 4. As seen in Fig. 4, by decreasing the porosity a significant reduction in the two-phase region occurs. Notice that for $\gamma=0.95$ the apparent critical pressure of the confined mixture is now decreased by about 50% compared to the bulk phase mixture, while the overall phase envelope for $\gamma=0.95$ is shifted to slightly higher values of x_1. This behavior can be attributed mainly to the relative strengths of the mixture components ($\varepsilon_{11}>\varepsilon_{22}$); the stronger cohesive interactions between species-1 particles adsorbed in the pores tend to drive out species-2 particles. The phase coexistence curves for both porosities exhibit similar reductions in the liquid-phase composition of species 1. However, the composition of species 1 in the vapor phase for $\gamma=0.975$ appears to have shifted to slightly lower values, while for $\gamma=0.95$ x_1 has increased.

The third mixture (mixture III) is intended to study both size and energetic effects on the phase envelope. Mixture III has the same energy parameters as mixture II but the size of species 2 is reduced to $\sigma_{22}=0.75$. The phase diagrams were determined for porosities of $\gamma=0.95$ and 0.9 at $T^*=0.75$. Again the confined fluid phase diagram exhibits considerable deviations from the bulk fluid phase diagram. The pressure-composition and pressure-density coexistence curves for $\gamma =0.95$ are shown in Figs. 5(a) and 5(b), respectively. As expected, the overall reduction and shape of the phase envelopes are similar to those of mixture II. Interestingly, the critical pressure of the confined mixture appears to be higher than the critical pressure of the corresponding bulk fluid. Shifts in the confined fluid phase diagrams shown in Figs. 3–5 (i.e., the liquid phase moves to lower densities while the vapor phase density remains nearly the same) are similar to those exhibited for pure fluids in similar porous solid models. The behavior is indicative of a repulsive material where the solid particles "discourage" occupation of pores except for smaller sized molecules [5]. In Fig. 6, we show the

(a)

(b)

FIG. 5. Pressure-composition (a) and pressure-density (b) phase diagrams for mixture III at $T^*=0.75$. The porosity of the solid structure is $\gamma=0.95$. Further details are the same as in Fig. 3.
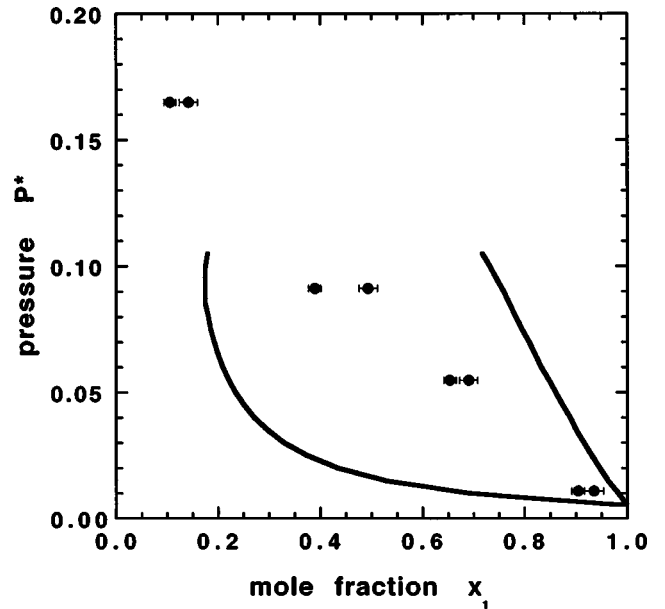

FIG. 6. Pressure-composition phase diagram for mixture III at $T^*=0.75$ and $\gamma=0.9$. Further details are the same as in Fig. 2.

$=0.9$. However, phase separation did not occur for any of the mixtures. This may be partly due to the lack of a significant number of large pores present in our porous model (recall that $\sigma_s=\sigma_{11}$).

Finally, it should be noted that only one realization of the porous structure was used for each phase envelope generated in this work. Recent findings indicate a strong dependence of the phase behavior on the particular realization of the porous structure[3–5], which may also be partly due to finite size effects. In this study, system sizes were increased until the calculated quantities converged, requiring cell lengths that (relative to comparable bulk fluid simulations) are fairly large ($12\sigma_{11}-15\sigma_{11}$). Further, simulations for different realizations of the porous structures used in this study are under way.

pressure-composition phase diagram for mixture III at a decreased porosity of $\gamma=0.9$. Note the dramatic narrowing of the two-phase region compared to Fig. 5(a) and the further increase of the critical pressure for the mixture.

The simulated phase coexistence curves reported in this work reasonably bound the two-phase region for these mixtures. Constant-pressure Gibbs ensemble simulations performed at pressures a few percent outside the bounds shown in the plots did not exhibit two-phase behavior. Notwithstanding, the phase diagrams reported here are intended to establish trends for these model systems rather than the calculation of highly accurate coexistence curves. We also note that attempts were made to determine two-phase fluid behavior for our porous solid model at porosities lower than γ

IV. CONCLUSIONS

In this work, we studied the vapor-liquid phase behavior of a few simple mixtures in randomly disordered porous solid. The pressure-density and pressure-composition phase diagrams have been presented for three different Lennard-Jones mixtures. Despite using highly porous structures in this study, we found dramatic shifts and reductions in the phase envelope. We found both the size and energetic characteristics of the fluid mixture to be critical elements in understanding the phase behavior of fluids in confinement. Furthermore, for the binary mixtures studied here we were unable to locate two-phase regions for porosities lower than $\gamma=0.9$. For porous models with attractive character, one would not expect the reduction of the overall two-phase region to be as prevalent at these porosities. However, one would expect more dramatic shifts in the pressure-composition phase diagram due to selective adsorption or preferred orientation of mixture components with the porous material.

The role of this work is twofold. First, it is an initial step

in understanding the fundamental issues of these complex phenomena. However, further similar studies are essential to categorizing behavioral trends. Furthermore, such studies can play a critical role in the development of theoretical models. Simulation studies supply much needed data for the development and refinement of theoretical models by providing essentially exact results (within statistical uncertainty) for the model considered.

Lastly, while fundamental studies are needed it would be interesting to simulate the phase behavior of fluid mixtures in realistic porous materials, e.g., the activated carbon models currently being developed [13,14]. Adsorption studies of po-lar molecules in these models have shown dramatic effects on the adsorption isotherms due to the connectivity of the pore structure [15]. Phase equilibria studies may provide further insight into this phenomenon.

ACKNOWLEDGMENTS

[1] A. P. Y. Wong and M. H. W. Chan, Phys. Rev. Lett. **65**, 2567 (1990).

[2] K. S. Page and P. A. Monson, Phys. Rev. E **54**, 6557 (1996).

[3] M. Alvarez, D. Levesque, and J-J. Weiss, Phys. Rev. E **60**, 5495 (1999).

[4] L. Sarkisov and P. A. Monson, Phys. Rev. E **61**, 7231 (2000).

[5] J. K. Brennan and W. Dong, J. Chem. Phys. **116**, 8948 (2002).

[6] D. M. Ford and E. D. Glandt, Phys. Rev. E **50**, 1280 (1994).

[7] J. K. Johnson, J. A. Zollweg, and K. E. Gubbins, Mol. Phys. **78**, 591 (1993).

[8] A. Z. Panagiotopoulos, N. Quirke, M. Stapleton, and D. J. Tildesley, Mol. Phys. **63**, 527 (1988).

[9] M. P. Allen and D. J. Tildesley, *The Computer Simulation of Liquids* (Clarendon, Oxford, 1991), Chap. 1, p. 24ff, Chap. 6, p. 192.

[10] D. Frenkel and B. Smit, *Understanding Molecular Simulation* (Academic, San Diego, 2002), Chap. 3, p. 32ff.

[11] V. I. Harismiadis, N. K. Koutras, D. P. Tassios, and A. Z. Panagiotopoulos, Fluid Phase Equilibria **65**, 1 (1991).

[12] J. P. Hansen and I. R. McDonald, *Theory of Simple Liquids* (Academic, London, 1971).

[13] K. T. Thomson and K. E. Gubbins, Langmuir **16**, 5761 (2000).

[14] J. Pikunic, C. Clinard, N. Cohaut, K. E. Gubbins, J.-M. Guet, R. J.-M. Pellenq, I. Rannou, and J.-N. Rouzaud, in *Proceedings of the 6th International Symposium on the Characterization of Porous Solids*, edited by F. Rodriguez-Reinoso, B. McEnaney, J. Rouquerol, and K. K. Unger (Elsevier, Amsterdam, 2002), pp. 16–26.

[15] J. K. Brennan, K. T. Thomson, and K. E. Gubbins, Langmuir **18**, 5438 (2002).